Bidimensional Particle-In-Cell simulations for laser-driven proton acceleration using ultra-short, ultra-high contrast laser

M. Scisciò,[1] E. D'Humières,[2] S. Fourmaux,[3] J. C. Kieffer,[3] L. Palumbo,[1] and P. Antici[1,3,4,a)]
[1]*Dipartimento SBAI, Sapienza, Università di Roma, Via Scarpa 16 and INFN-RM, 00161 Roma, Italy*
[2]*University of Bordeaux, CNRS-CEA, CELIA, UMR5107, 33405 Talence, France*
[3]*INRS-EMT, Université du Québec, 1650 Lionel Boulet, Varennes J3X 1S2, Québec, Canada*
[4]*ELI-ALPS, Dugonics ter 13, 6720 Szeged, Hungary*

(Received 17 July 2014; accepted 1 November 2014; published online 4 December 2014)

In this paper, we report on bi-dimensional Particle-In-Cell simulations performed in order to reproduce the laser-driven proton acceleration obtained when a commercial 200 TW Ti:Sa Laser hits a solid target. The laser-to prepulse contrast was enhanced using plasma mirrors yielding to a main-to-prepulse contrast of $\sim 10^{12}$. We varied the pulse duration from 30 fs to 500 fs and the target thickness from 30 nm to several tens of μm. The on-target laser energy was up to 1.8 J leading to an intensity in excess of 10^{20} W cm^{-2}. A comparison between numerical and existing experimental data [S. Fourmaux *et al.*, Phys. Plasmas **20**, 013110 (2013)] is performed, showing a good agreement between experimental results and simulations which confirms that for ultra-thin targets there is an optimum expansion regime. This regime depends on the target thickness and on the laser intensity: if the target is too expanded, the laser travels through the target without being able to deposit its energy within the target. If the target is not sufficiently expanded, the laser energy is reflected by the target. It is important to note that maximum proton energies are reached at longer pulse durations (in the 100 fs regime) than what is currently the best compression pulse length for this type of lasers (typically 20–30 fs). This duration, around 50–100 fs, can be considered a minimum energy transfer time between hot electrons to ions during the considered acceleration process.
 [http://dx.doi.org/10.1063/1.4902125]

I. INTRODUCTION

Since more than a decade, intense research is being conducted on laser-accelerated ion sources using short-pulse high-intensity lasers. Laser-generated ions, achieving nowadays energies in the tens of MeV regime, have shown to be of very low emittance,[1] low divergence,[2] and short bunch duration, therefore enabling many innovative applications such as ultrafast radiography and isochoric heating (Warm dense matter).[3–5] However, for many applications, e.g., in the medical field, such as in the medical field, the maximum ion energy and the maximum ion flux are still too low. Scaling laws indicate[6–8] that the maximum proton energy heavily depends on the laser energy and by consequence that the constant improvements on laser technology (achieving currently focused intensities of up to $\sim 10^{21}$ W cm^{-2}) could open the way for generating laser-driven particle sources that can potentially complement and outperform conventional, electromagnetic field-based, accelerators. In particular, the flexibility, reduced size, and hence lower costs of laser systems compared to conventional accelerator facilities are strongly in favor of developing laser-generated accelerators.

Up to now, highest ion energies, in excess of 65 MeV, have been obtained with high-energy high-power lasers operating in a single shot mode, i.e., a shot every tens of minutes or more, although higher energies have been claimed recently by novel acceleration mechanisms (BOA).[9] Driven by the requirements of higher flux and higher ion energy, industry and applied science laser centres are, however, commercializing and designing more and more laser systems going towards higher repetition rate and higher energies: today, many commercial table-top laser systems in the hundreds of TW regime deliver energies of up to a few J in 25–30 fs with a repetition rate of up to 10 Hz. Some of these systems are about to be upgraded to the Petawatt level (e.g., the VEGA system in Salamanca, the DRACO Laser in Dresden, CETAL Laser in Romania) or even to the tens of PW level (such as the Extreme Light Infrastructure), increasing the energy, but keeping the pulse duration in the same range. These short-pulse high-repetition rate systems are different from the single-shot laser facilities (mostly custom-made) mentioned above. Even if the latter laser systems are reaching the same intensity, they are doing so by using a longer pulse (>500 fs) and higher energy (>100 J). They are therefore considered to be more appropriate for fusion studies and research on this topic is conducted on laser systems such as the TRIDENT laser facility (located at the LANL laboratory) or the PETAL laser facility (located at the CESTA site of CEA).[10–12]

There have been extensive studies about proton generation using different laser systems. In particular, concerning short-pulse and high-repetition rate laser systems in the 100 TW regime, most of them commercial—achieving ~5 J with laser pulses of 25–30 fs—different research groups have measured proton energies going routinely up to 15 MeV.[8,13,14] These protons are obtained with the most-known standard acceleration regime, the Target Normal Sheath Acceleration (TNSA)[15] acceleration mechanism. In this regime, acceleration of protons

a)Electronic mail: patrizio.antici@polytechnique.edu

from a solid target irradiated by a high-intensity laser pulse occurs in a two-step mechanism: the laser-matter interaction generates energetic (hot) electrons at the front surface with a mean free path longer than the standard target thickness. Electrons propagate through the target and establish at its rear target surface a space-charge sheath field in the TV/m regime that accelerates protons from contaminants (e.g., water residual) located on the external surfaces. Without any special cleaning of the target surface, protons are the main ion species that is accelerated due their higher charge-to-mass ratio.[16] The generation of high-energy ions can be favored by pre-heating the target in order to clean it from the contaminants.[9]

Proton acceleration on the shorter-pulse high-repetition laser systems has been reported with μm[8,14] and sub μm solid targets.[13,17] Ultra-thin (i.e., sub-micrometric) targets, typically <0.5 μm thick, enable a more efficient hot electron production compared to thicker targets.[18,19] Since the thickness of the target is of the same order of magnitude than the laser penetration depth into the material, hot electrons are generated within the entire volume of the target. Unfortunately, very thin targets put crucial constraints on the contrast of the laser pulse, i.e., the ratio between the amplitude of the main pulse and the preceding laser-light pedestal, sometimes also refereed as Amplified Spontaneous Emission (ASE): a too intense pre-pulse can alter the target's planarity (or even destroy the target) before the main pulse arrives, leading to a worse acceleration mechanism.[20]

In this paper, we report on maximum proton energies using sub-micrometric plain targets and being irradiated by a commercial short-pulse high-repetition rate laser, where the laser contrast has been enhanced using a plasma mirror. We focused in the current paper on plain solid target foils in order to reproduce the experimental conditions, although we are aware that other targets have been used to enhance the proton acceleration, e.g., using microstructured, nanostructured, and foam targets.[21–26] A laser-to-prepulse contrast of 10^{12} up to 20 ps before the main pulse, i.e., two orders of magnitude higher than without the plasma mirror, has been achieved. At 1 ps before the main-pulse, the laser has typically a contrast ratio of 10^5, we can thus expect a contrast improvement of about 10^7 with the plasma mirror. The reflectivity of the plasma mirror has been measured during the experiment and is about 60% for the laser pulse at nominal energy (and only of 0.5% for low-intensity laser light), which leads to an energy delivered on the target of 1.8 J.[13]

From Ref. 13, experimental evidence shows how there is an optimum value for the laser pulse duration, in order to achieve the highest proton energy: At a fixed laser energy of 1.8 J, irradiating the target with a laser pulse of $\sim$100 fs yields a cut-off energy of nearly 12 MeV for the protons accelerated at the front surface of the target. Such high energies could not be obtained with other pulse durations (both shorter and longer) when keeping the laser energy at a constant value.[13]

We show that simulations reproduce the experimental behavior of laser-acceleration using short-pulse irradiation and we confirm that there is an optimum pulse duration for which the proton acceleration is enhanced. This optimum is due to a compromise condition between the fact that the expansion of the target increases the absorption, and the fact that the density needs to remain high enough in order to avoid that the laser goes through it without depositing energy.

II. SETUP

The experimental setup considered for the simulations is shown in Fig. 1 and described in Ref. 13: The laser irradiates solid targets of various thickness (from 30 nm to 1 μm) with an angle of 45° generating on target intensities of up to 10^{20} W cm^{-2} for the shortest pulse duration of 30 fs with a gaussian laser profile. The laser has a wavelength of 800 nm and is focused down to a gaussian spot-size with diameter of 5.6 ± 0.4 μm Full-Width-Half-Max (FWHM). The laser-to-prepulse contrast without the correction of the plasma mirrors is in the order of 10^{10} and using one Plasma Mirror, it is in excess of 10^{12} (up to 20 ps before the main pulse).

Simulations were performed using the PIC code PICLS-2D, well suited for simulating high density plasmas since covering a wide range of regimes (cold, non-relativistic up to ultra-relativistic regimes, which are typical of high-energy-density physics (HEDP)).[27] For the simulations, we concentrated only on solid foil targets of 120 nm thickness (manufactured by a layer of 30 nm Si_3N_4 covered with 90 nm Al), since the best experimental results had been obtained for this target. The laser was impinging the target from the Al-surface side.

In order to decipher the acceleration process, we retrieved information about the spectral distribution of the proton energy (and its cut-off energy) and on the reflectivity of the target. The latter can be measured indirectly by monitoring the ratio between the electromagnetic energy within

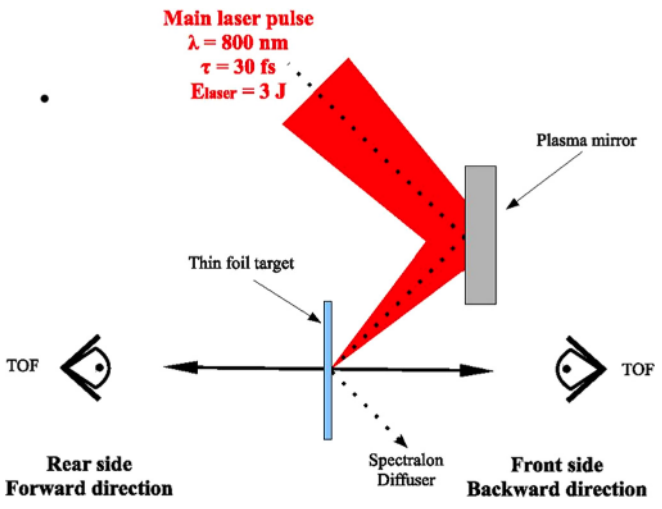

FIG. 1. Experimental setup depicted in the laser plane-of-incidence. The main laser pulse is incident at 45°, on both the plasma mirror and the target, P-polarized for both. Charged-particle TOF diagnostics are positioned on the target surface normal-axis, measuring both front- and rear-side accelerated proton beams. The target reflectivity is measured with the help of a Spectralon diffuser located in the specular beam path. Setup extracted from Ref. 13. Reprinted with permission from Fourmaux *et al.*, Phys. Plasmas **20**, 013110 (2013). Copyright (2013) American Institute of Physics.

the simulation box and the energy transferred to the particles within the target that is accelerated. We investigated the kinetic energy of the protons in two ways: (1) varying the pulse lengths from 30 fs up to 300 fs (FWHM), keeping the energy of the laser constant at $E_{laser} = 1.8\,\mathrm{J}$, and (2) with a fixed pulse length of 30 fs, but varying the intensity (from $10^{19}\,\mathrm{W\,cm^{-2}}$ to $10^{20}\,\mathrm{W\,cm^{-2}}$) and therefore the pulse energy from 200 mJ to 1800 mJ. For both cases, the simulated laser beam had a spot-size of 5.6 μm.

We run the simulations using a spatial resolution of 4 nm for both x- and y-direction and a time resolution of 0.0135 fs, which gave us sufficient resolution to follow the electromagnetic behavior of the particles during the simulation. The target bulk is simulated with fully ionized Al particles, whereas a layer of 8 nm protons is put at the external surfaces of the target itself. We considered perfectly planar surfaces, making the hypothesis that the very high contrast of our laser (10^{12}) does not create a pre-plasma gradient that would notably affect the laser absorption. We used two different electron densities n_e in order to simulate the double layer target, respectively, $n_e(Al) \approx 77 n_{cr}$ for Aluminium and $n_e(Si_3N_4) \approx 132 n_{cr}$ for silicon-nitride, where the optical critical density n_{cr} is defined as

$$n_{cr}\,[\mathrm{cm^{-3}}] \approx \frac{1.1 \times 10^{21} \times \cos(\alpha)}{\lambda^2_{laser}[\mu\mathrm{m}]}$$

with α the incidence angle of the laser pulse and λ_{laser} the laser wavelength.

The simulated laser pulse spot-size has a diameter of 5.6 μm with gaussian shape. Collisions between particles were neglected, since we have seen that in these conditions collisions do not significantly alter the results.[18]

III. COMPARISON OF NUMERICAL SIMULATIONS WITH EXPERIMENTAL DATA

At first, we analyse the particle energy evolution over the entire simulation, including the associated electromagnetic fields. An example of energy balance in time, when using as pulse duration a gaussian pulse of 100 fs, can be seen in Fig. 2. The green curve reports the density of the electromagnetic energy within the grid; the purple, red, and light-blue curves indicate the kinetic energy density of all simulated particles (electrons, protons, and aluminum-ions, respectively); the blue curve identifies the total energy density of the system.

We can see a delay of ~60 fs between the peak of the purple ($t \approx 210$ fs) and green curve ($t \approx 150$ fs, indicating the electromagnetic source in our system), which is approximately equal to the time that it takes for the laser to transfer its energy to the hot electrons. We also see that there is a delay between the peak of the electron and proton energy compared to the total laser energy. This is due to the fact that the laser energy takes some time to transfer its energy to the ions and electrons. However, we see that the energy transfer for both particles starts almost at the same time (30 fs later for both). From the slow onset of the proton energy density, it would seem that a consistent recirculation is needed in order to setup the acceleration process.

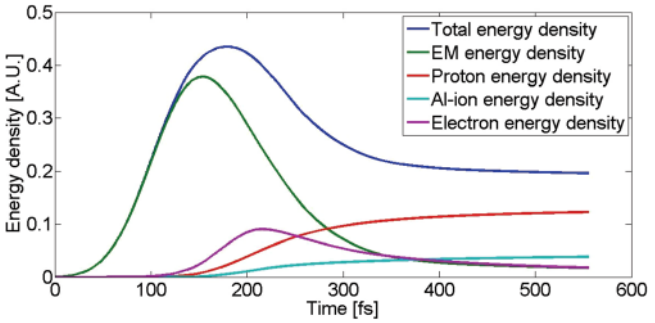

FIG. 2. Energy density within the simulation box versus elapsed time from the beginning of the simulation. The temporal profile of the incident laser pulse is gaussian with a FWHM of 100 fs. From the green curve, we can estimate that the peak of the laser pulse is at $t \approx 150$ fs. On the ordinate axis, we have a normalized unit, expressing the indicated energy as fraction of the total amount of energy of particles and electromagnetic fields averaged over the bi-dimensional simulation box. The origin on the time axis is related to the beginning of the simulation, about 150 fs before the laser pulse peak.

We can estimate the reflectivity of the target to be approximately the following ratio: the difference between peak of the electromagnetic energy density within the box (green curve) and the final, stabilized energy of all the particles (i.e., when no more energy is exchanged between the laser's electromagnetic field and the particles), divided by the peak of the electromagnetic energy density. It reads $R = (ED_{EM} - ED_{part})/ED_{EM}$, where R is the fraction of the reflected energy, ED_{EM} is the electromagnetic energy density, and ED_{part} is the final energy density stored in the particles. In the current case, this is achieved after ~450 fs. This value corresponds to 4.5 times the laser pulse duration and is consistent with the fact that for shorter laser pulses, the ratio $\frac{stabilizing-time}{pulse-duration}$ (in our case ≈4.5) is higher than for longer pulses, were a factor 1.3 had been estimated.[6,28] The target reflectivity deduced with the above mentioned method for different pulse durations (from 30 fs to 300 fs) is reported in Fig. 3. For all these simulations, the laser energy has been kept constant at $E_{laser} = 1.8\,\mathrm{J}$ (the intensity of the pulse is inversely proportional to the pulse duration).

We see in Fig. 3 that the reflectivity decreases from ~74% for the 30 fs pulse to ~45% for the 300 fs pulse, which confirms that for less ionized/exploded targets (such as produced when irradiating the target with the 30 fs laser), the reflectivity is much higher than when the target has time to decompress. What is interesting to note is that in the timeframe 60–150 fs, the reflectivity stays almost constant (~52%–59%) and the use of ultra-thin targets and high-contrast lasers requires longer pulses in order to improve and increase the absorption, as already confirmed by other experiments.[18,29,30] The small reflectivity peak at 120 fs is to be considered a fluctuation of the values to be found in the interval between 100–150 fs. Looking on other parameters of the simulation, we find that the energy absorption for this case is slightly lower, which would justify the higher reflectivity, but is still comparable with what is found for the other values of time.

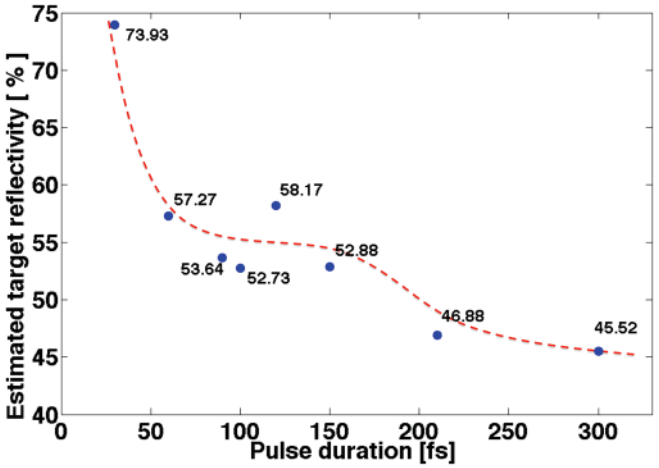

FIG. 3. Target reflectivity as a function of the laser pulse duration. The red dashed line is a guide for the eye.

A typical proton spectrum, as computed with the PIC code, is shown in Figure 4. The pulse duration is ~100 fs and the intensity is $I_{laser} = 0.3 \times 10^{20}$ W cm^{-2}. The spot-size of the impinging laser is ~5.6 μm with an incidence angle of 45°. The target thickness is 120 nm. We see that the spectrum is Maxwellian with a cutoff-energy of 14 MeV, slightly more than what was found experimentally. The acceleration process is almost symmetric with a slight improvement in maximum achievable energy at the front surface. This is due to the fact that the rear target surface is more perturbed by the impinging laser pulse during the acceleration process. Considering the absolute value of the protons, the simulations overestimate the proton yield, likely due to the fact that the 2D simulations do not take into account 3D effects during the expansion process. Moreover, the number of particles of the experimental spectra is almost one order of magnitude lower than what typically achieved on longer pulse, higher energy laser, were at lower energies routinely up to 10^{12} particles/MeV can be obtained.

Figure 5 compares the maximum proton energy obtained for different intensities and for both, simulations and experiment (experimental values are taken from Fourmaux *et al.*[13]). One can identify a trend for the proton energy that scales with the square root of the pulse intensity, such as found in Ref. 6 or Ref. 7 and that reads: $E[MeV] \approx 2.9 \cdot \sqrt{I_{laser}}$ with laser intensity in units of 10^{19} W/cm^2.

This fit is applicable for the rear side and front side target protons and confirms that for the present acceleration regime, as expected, we are still in TNSA, although intensity is reaching values, where new acceleration regimes should start to become active.

Figures 6 and 7 compare experimental and numerical results for the case with fixed energy of the laser and varying pulse duration. The maximum proton energy shows a pronounced peak of 11 MeV (for the experimental results) for pulse durations in the order of 100 fs whereas before and after it reaches 8 MeV.

In Figures 5–7, simulations correctly reproduce the experimental trend. The slight overestimation of the maximum proton energy by the simulations (up to 40% higher values in the cases with 60 fs, 90 fs, and 100 fs), which can be identified in both cases, with both fixed and varying pulse duration, is due to the fact, that simulations are 2D (and not 3D). This leads to emphasized maximum proton energies with respect to the real (3D) scenario. This issue and a consequent adjustment have been proposed by Margarone *et al.*,[22] adapting the spot-size of the laser pulse from its original size in the 2D simulations. The lateral losses are only one directional in the 2D geometry used in the simulations. Thus, they are reduced compared to the experiment. In order to compensate this reduction, a smaller focal spot shall be used in 2D simulations. Simulations run with the adjusted size of the focal spot, i.e., with a diameter of ~3.68 μm, gave a reduced cut-off energy for the proton beam simulations (maximum energy is ~11 MeV for the front surface and ~10 MeV for the rear side in the case of a 100 fs long pulse), which matches better with the experimental data. The following figures and the spectra of Figure 4 show simulation results obtained using an unaltered spot-size (~ 5.6 μm diameter).

In both acceleration mechanisms (front and rear target surfaces), there is an optimum for pulse lengths between 60 fs and 100 fs even in the case when the total laser energy is fixed for all pulse durations. For these conditions, there is the best interplay between different scenarios: (1) if the

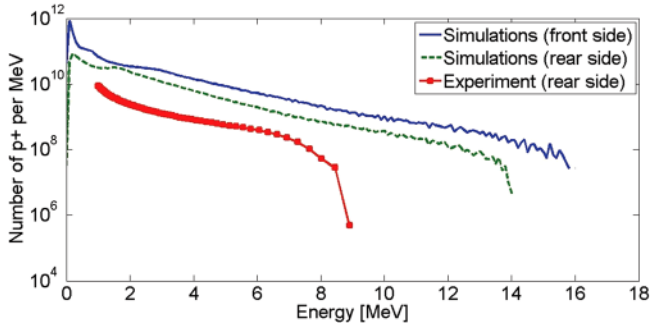

FIG. 4. Energy spectra of protons accelerated on the front (blue, solid) and rear (green, dashed) surface of the target by a 100 fs long pulse with $I_{laser} = 0.3 \times 10^{20}$ W cm^{-2}. The target thickness is 120 nm. When interpreting the numerical spectra, we took the beginning of the noisy part of the spectrum as lowest maximum proton energy and the end of the spectrum as maximum. The cut-off energy is considered to be the mean value of both and the associated error-bars the relative distances. The red curve with rectangular markers represents the experimental values for rear-side acceleration under the same circumstances as simulations.

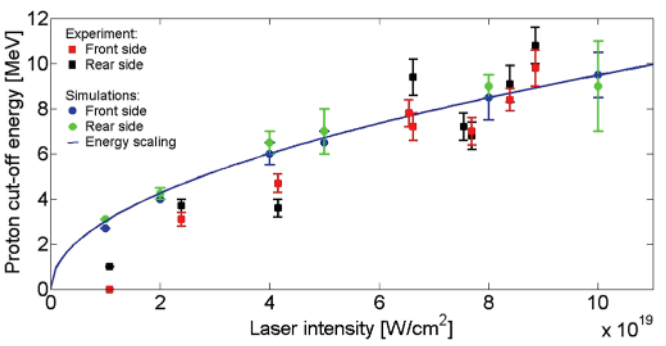

FIG. 5. Comparison between experimental and simulations' data for proton cut-off energy vs. laser intensity. The pulse duration is fixed at 30 fs, the spot-size of the impinging laser is 5.6 μm (FWHM) and the pulse energy varies from 200 mJ to 1.8 J. The blue curve represents a fit for numerical data, for the rear-surface acceleration.

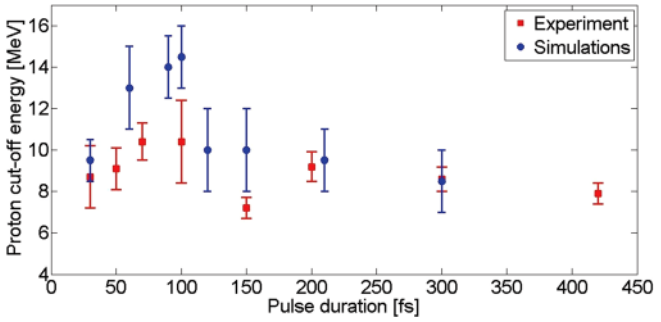

FIG. 6. Comparison between experimental and simulations' data for proton acceleration on the front side of the target (cut-off energy vs. pulse duration). The energy of the laser pulse is constant as $E_{laser} = 1.8$ J.

target is sufficiently decompressed, it can best absorb the laser energy; (2) if the target is too diluted, the laser pulse goes through it without depositing its energy; (3) if the target is not sufficiently decompressed, the laser energy is reflected by the steep target gradient. This is similar to what has already been identified by Refs. 14 and 29.

IV. DATA INTERPRETATION: DECIPHERING THE ACCELERATION MECHANISM

We compare the maximum proton energy of a 100 fs pulse and a 210 fs pulse in order to see how the external layers on the solid target's surfaces expand and/or are damaged by the laser pulse. Figures 8 and 9 show the proton phase space at ~122 fs and ~216 fs after the start of the simulation, for these two cases, respectively. For the first case, the snapshot is taken at the time when the peak of the pulse has reached the front surface of the foil. We notice how the two proton layers are still planar and only little expansion has occurred: this corresponds to the instant of time when the proton acceleration process is starting, as can be confirmed from the related energy evolution diagram (Figure 2). The presence of an expanding plasma on the target's surface (rear and front) is a crucial parameter in the TNSA mechanism. Indeed, the charge separation, which drives the proton acceleration, is proportional to $(n_{hot} \times T_{hot})^{1/2}$ when the plasma scale length l_g is below the hot electron Debye length λ_d.[31] However, it is reduced to $\frac{T_{hot}}{l_g}$ when $l_g > \lambda_d$.[28,32] This is the case for long laser pulse durations, which induce longer plasma gradients. The density map of Figure 9 pictures the

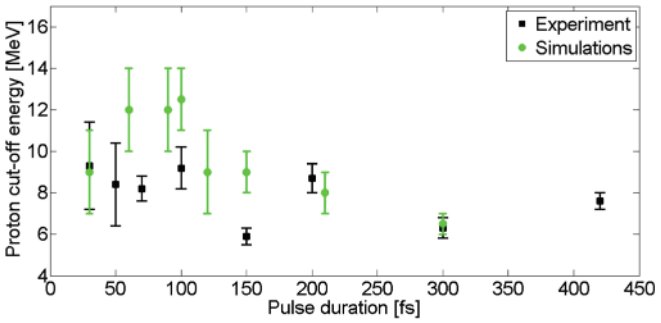

FIG. 7. Comparison between experimental and simulations' data for proton acceleration on the rear side of the target (cut-off energy vs. pulse duration). The energy of the laser pulse is constant as $E_{laser} = 1.8$ J.

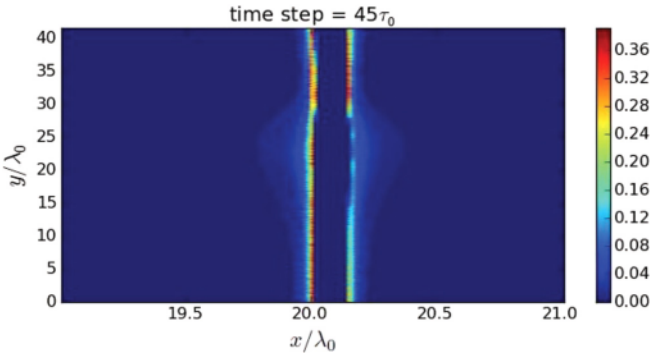

FIG. 8. Density map of protons for the 100 fs pulse case. The target is seen from the side with x being the longitudinal direction and y the radial. X and Y units are normalised to the laser wavelength. The density is given as normalized to the maximum density (here, $\sim 132 \times n_{cr}$).

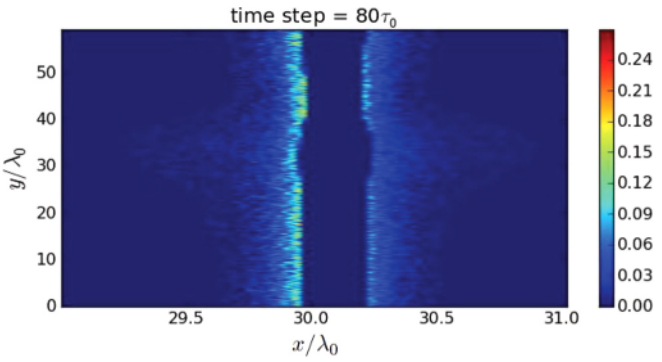

FIG. 9. Density map of protons for the 210 fs pulse case. The target is seen from the side with x being the longitudinal direction and y the radial. X and Y units are normalised to the laser wavelength. The density is given as normalized to the maximum density (here, $\sim 132 \times n_{cr}$).

situation at a moment when the peak of the laser pulse has still not reached the target completely. For this second case, the boundary proton layers appear to be much more expanded and the planarity of the targets is significantly worse than in the previous case: although it is still acceptable to enable ion acceleration, it is not as optimized as the previous case. This demonstrates how the later part of a long laser pulse has rather a worsening effect on the acceleration process than enhancing it. Therefore, we must deduce that shorter laser pulses deliver their energy to the electrons earlier than this target degeneration occurs and that the accelerating charge-separation field at the target rear surface is created before the proton layers lose their planarity. This allows obtaining higher proton energies.

V. CONCLUSION

This paper completes the understanding of experimental data related to laser-driven proton acceleration obtained when a commercial 200 TW Ti:Sa laser pulse with enhanced laser-to-prepulse contrast hits a solid target. Based on numerical Particle-In-Cell simulations, we are able to understand the underlying physical mechanism for previously obtained experimental results. This allows having a better insight on the optimum experimental conditions for the acceleration regime: these conditions result from an interplay between

different scenarios: (1) if the target is sufficiently decompressed, it can best absorb the laser energy; (2) if the target is too diluted, the laser pulse travels through it without depositing its energy; (3) if the target is not sufficiently decompressed, the laser energy is reflected by the steep target gradient. Since these kind of laser-facilities are currently envisioned to be used for laser-driven proton applications, it is important to note that maximum proton energies are reached at longer pulse durations (100 fs regime) than what is currently the best compression pulse length (typically 20–30 fs). This can be considered a minimum energy transfer time between electrons to ions during the acceleration process. We focused in the current Ms on plain solid target foils, although other targets have been used to enhance the proton acceleration, e.g., using microstructured, nanostructured, and foam targets.[21–26] Our results can lead to the general conclusion that whenever using ultra-thin targets, optimization of the pulse's duration is required in order to maximize the acceleration process.

ACKNOWLEDGMENTS

This work was supported by the European Commission (CRISP FP-7 Contract No. 283745) and ELI-ITALY (P. Antici and M. Sciscio), FRQNT/FRQSC (Grant No. 174726) (P. Antici), CRSNG decouverte (Grant No. 435416), and ComputeCanada (Job: pve-323-ab, P. Antici).

[1]T. Cowan, J. Fuchs, H. Ruhl, A. Kemp, P. Audebert, M. Roth, R. Stephens, I. Barton, A. Blazevic, E. Brambrink, J. Cobble, J. Fernandez, J.-C. Gauthier, M. Geissel, M. Hegelich, J. Kaae, S. Karsch, G. Le Sage, S. Letzring, M. Manclossi, S. Meyroneinc, A. Newkirk, H. Pepin, and N. Renard- LeGalloudec, Phys. Rev. Lett. **92**(20), 204801 (2004).
[2]J. Fuchs, T. Cowan, P. Audebert, H. Ruhl, L. Gremillet, A. Kemp, M. Allen, A. Blazevic, J.-C. Gauthier, M. Geissel, M. Hegelich, S. Karsch, P. Parks, M. Roth, Y. Sentoku, R. Stephens, and E. Campbell, Phys. Rev. Lett. **91**(25), 255002 (2003).
[3]A. Mancic, J. Robiche, P. Antici, P. Audebert, C. Blancard, P. Combis, F. Dorchies, G. Faussurier, S. Fourmaux, M. Harmand, R. Kodama, L. Lancia, S. Mazevet, M. Nakatsutsumi, O. Peyrusse, V. Recoules, P. Renaudin, R.Shepherd, and J. Fuchs, High Energy Density Phys. **6**, 21–28 (2010).
[4]P. Antici, J. Fuchs, S. Atzeni, A. Benuzzi, E. Brambrink, M. Esposito, M. Koenig, A. Ravasio, J. Schreiber, A. Schiavi, and P. Audebert, J. Phys. IV France **133**, 1077–1079 (2006).
[5]P. K. Patel, A. J. Mackinnon, M. H. Key, T. E. Cowan, M. E. Foord, M. Allen, D. F. Price, H. Ruhl, P. T. Springer, and R. Stephens, Phys. Rev. Lett. **91**(12), 125004 (2003).
[6]J. Fuchs, P. Antici, E. D'Humieres, E. Lefebvre, M. Borghesi, E. Brambrink, C. A. Cecchetti, M. Kaluza, V. Malka, M. Manclossi, S. Meyroneinc, P. Mora, J. Schreiber, T. Toncian, H. Pepin, and P. Audebert, Nat. Phys. **2**(1), 48–54 (2006).
[7]L. Robson, P. T. Simpson, R. J. Clarke, K. W. D. Ledingham, F. Lindau, O. lund, T. McCanny, P. Mora, D. Neely, C.-G. Wahlstrom, M. Zepf, and P. McKenna, Nat. Phys. **3**, 58–62 (2007).
[8]K. Zeil, S. D. Kraft, S. Bock, M. Bussmann, T. E. Cowan, T. Kluge, J. Metzkes, T. Richter, R. Sauerbrey, and U. Schramm, New J. Phys. **12**, 045015 (2010).
[9]B. M. Hegelich, D. Jung, B. J. Albright, M. Cheung, B. Dromey, D. C. Gautier, C. Hamilton, S. Letzring, R. Munchhausen, S. Palaniyappan, R. Shah, H.-C. Wu, L. Yin, and J. C. Fernndez, see http://arxiv.org/abs/1310.8650.
[10]G. A. Mourou, C. L. Labaune, M. Dunne, N. Naumova, and V. T. Tikhonchuk, Plasma Phys. Controlled Fusion **49**, B667–B675 (2007).
[11]N. Blanchot, G. Behar, T. Berthier, E. Bignon, F. Boubault, C. Chappuis, H. Coic, C. Damiens-Dupont, J. Ebrardt, Y. Gautheron, P. Gibert, O. Hartmann, E. Hugonnot, F. Laborde, D. Lebeaux, J. Luce, S. Montant, S. Noailles, J. Neauport, D. Raffestin, B. Remy, A. Roques, F. Sautarel, M. Sautet, C. Sauteret, and C. Rouyer, Plasma Phys. Controlled Fusion **50**, 124045–10 (2008).
[12]K. A. Flippo, E. d'Humieres, S. A. Gaillard, J. Rassuchine, D. C. Gautier, M. Schollmeier, F. Nuernberg, J. L. Kline, J. Adams, B. Albright, M. Bakeman, K. Harres, R. P. Johnson, G. Korgan, S. Letzring, S. Malekos, N. Renard-LeGalloudec, Y. Sentoku, T. Shimada, M. Roth, T. E. Cowan, J. C. Fernandez, and B. M. Hegelich, Phys. Plasmas **15**, 056709 (2008).
[13]S. Fourmaux, S. Buffechoux, B. Albertazzi, D. Capelli, A. Levy, S. Gnedyuk, L. Lecherbourg, P. Lassonde, S. Payeur, P. Antici, H. Pepin, R. S. Marjoribanks, J. Fuchs, and J. C. Kieffer, Phys. Plasmas **20**, 013110 (2013).
[14]A. Flacco, F. Sylla, M. Veltcheva, M. Carrie, R. Nuter, E. Lefebvre, D. Batani, and V. Malka, Phys. Rev. E **81**(3), 036405 (2010).
[15]S. C. Wilks, A. B. Langdon, T. E. Cowan, M. Roth, M. Singh, S. Hatchett, M. H. Key, D. Pennington, A. MacKinnon, and R. A. Snavely, Phys. Plasmas **8**(2), 542 (2001).
[16]S. J. Gitomer, R. D. Jones, F. Begay, A. W. Ehler, J. F. Kephart, and R. Kristal, Phys. Fluids **29**(8), 2679–2688 (1986).
[17]A. Henig, S. Steinke, M. Schnurer, T. Sokollik, R. Horlein, D. Kiefer, D. Jung, J. Schreiber, B. M. Hegelich, X. Q. Yan, J. Meyer-ter-Vehn, T. Tajima, P. V. Nickles, W. Sandner, and D. Habs, Phys. Rev. Lett. **103**, 245003 (2009).
[18]P. Antici, J. Fuchs, E. D'Humieres, E. Lefebvre, M. Borghesi, E. Brambrink, C. A. Cecchetti, S. Gaillard, L. Romagnani, Y. Sentoku, T. Toncian, O. Willi, P. Audebert, and H. Pépin, Phys. Plasmas **14**, 030701 (2007).
[19]T. Ceccotti, A. Levy, H. Popescu, F. Reau, P. d'Oliveira, P. Monot, J. P. Geindre, E. Lefebvre, and P. Martin, Phys. Rev. Lett. **99**(18), 185002 (2007).
[20]E. d'Humieres, J. L. Feugeas, P. Nicolai, S. Gaillard, T. Cowan, Y. Sentoku, and V. Tikhonchuk, J. Phys.: Conf. Ser. **244**, 042023 (2010).
[21]H. Schwoerer, S. Pfotenhauer, O. Jckel, K.-U. Amthor, B. Liesfeld, W. Ziegler, R. Sauerbrey, K. W. D. Ledingham, and T. Esirkepov, Nature **439**, 445–448 (2006).
[22]D. Margarone, O. Klimo, I. J. Kim, J. Prokapek, J. Limpouch, T. M. Jeong, T. Mocek, J. Pikal, H. T. Kim, J. Proka, K. H. Nam, L. Stolcov, I. W. Choi, S. K. Lee, J. H. Sung, T. J. Yu, and G. Korn, Phys. Rev. Lett. **109**, 234801 (2012).
[23]S. Okihara, T. Z. Esirkepov, K. Nagai, S. Shimizu, F. Sato, M. Hashida, T. Iida, K. Nishihara, T. Norimatsu, Y. Izawa, and S. Sakabe, Phys. Rev. E **69**, 026401 (2004).
[24]J. Zhang, Y. T. Li, Z. M. Sheng, Y. Y. Ma, Z. Jin, Z. L. Chen, R. Kodama, T. Matsuoka, M. Tampo, K. A. Tanaka, T. Tsutsumi, and T. Yabuuchi, Plasma Phys. Controlled Fusion **47**, B879 (2005).
[25]L. Willingale, S. R. Nagel, A. G. R. Thomas, C. Bellei, R. J. Clarke, A. E. Dangor, R. Heathcote, M. C. Kaluza, C. Kamperidis, S. Kneip, K. Krushelnick, N. Lopes, S. P. D. Mangles, W. Nazarov, P. M. Nilson, and Z. Najmudin, Phys. Rev. Lett. **102**, 125002 (2009).
[26]P. Antici, A. Mancic, M. Nakatsutsumi, P. Audebert, E. Brambrink, S. Gaillard, W. Nazarov, and J. Fuchs, Plasma Phys. Controlled Fusion **53**, 014002 (2011).
[27]Y. Sentoku and A. J. Kemp, J. Comput. Phys. **227**(14), 6846–6861 (2008).
[28]J. Fuchs, C. A. Cecchetti, M. Borghesi, T. Grismayer, E. D'Humieres, P. Antici, S. Atzeni, P. Mora, A. Pipahl, L. Romagnani, A. Schiavi, Y. Sentoku, T. Toncian, P. Audebert, and O. Willi, Phys. Rev. Lett. **99**, 015002 (2007).
[29]P. Antici, J. Fuchs, E. d'Humieres, J. Robiche, E. Brambrink, S. Atzeni, A. Schiavi, Y. Sentoku, P. Audebert, and H. Pepin, New J. Phys. **11**(2), 023038 (2009).
[30]D. Neely, P. Foster, A. Robinson, F. Lindau, O. Lundh, A. Persson, C.-G. Wahlstrom, and P. McKenna, Appl. Phys. Lett. **89**, 021502 (2006).
[31]P. Mora, Phys. Rev. Lett. **90**(18), 185002 (2003).
[32]T. Grismayer and P. Mora, Phys. Plasmas **13**(3), 032103 (2006).